# A flexible beamline combining XUV attosecond pulses with few-femtosecond UV and near-infrared pulses for time-resolved experiments ⊕

V. Wanie ✉ ⓘ ; S. Ryabchuk ⓘ ; L. Colaizzi ⓘ ; M. Galli ⓘ ; E. P. Månsson ⓘ ; A. Trabattoni ⓘ ;
A. B. Wahid ⓘ ; J. Hahne; A. Cartella ⓘ ; K. Saraswathula; F. Frassetto ⓘ ; D. P. Lopes;
R. Martínez Vázquez ⓘ ; R. Osellame ⓘ ; L. Poletto ⓘ ; F. Légaré ⓘ ; M. Nisoli ⓘ ; F. Calegari ⓘ

Check for updates

View Online

Export Citation

# A flexible beamline combining XUV attosecond pulses with few-femtosecond UV and near-infrared pulses for time-resolved experiments

View Online    Export Citation    CrossMark

V. Wanie,[1,a] S. Ryabchuk,[2,3] L. Colaizzi,[1,2] M. Galli,[1,4,5] E. P. Månsson,[1] A. Trabattoni,[1,6] A. B. Wahid,[1] J. Hahne,[2,3] A. Cartella,[1,3] K. Saraswathula,[1,2] F. Frassetto,[7] D. P. Lopes,[5] R. Martínez Vázquez,[4] R. Osellame,[4] L. Poletto,[7] F. Légaré,[8] M. Nisoli,[4,5] and F. Calegari[1,2,3]

## AFFILIATIONS

[1] Center for Free-Electron Laser Science CFEL, Deutsches Elektronen-Synchrotron DESY, 22603 Hamburg, Germany
[2] Department of Physics, Universität Hamburg, 22761 Hamburg, Germany
[3] The Hamburg Centre for Ultrafast Imaging, 22761 Hamburg, Germany
[4] Institute for Photonics and Nanotechnologies CNR-IFN, 20133 Milano, Italy
[5] Department of Physics, Politecnico di Milano, 20133 Milano, Italy
[6] Institute of Quantum Optics, Leibniz Universität Hannover, 30167 Hannover, Germany
[7] Institute for Photonics and Nanotechnologies CNR-IFN, 35131 Padova, Italy
[8] Centre Énergie Matériaux Télécommunications, Institut National de la Recherche Scientifique, J3X 1S2 Varennes, Canada

[a] Author to whom correspondence should be addressed: vincent.wanie@desy.de

## ABSTRACT

We describe a beamline where few-femtosecond ultraviolet (UV) pulses are generated and synchronized to few-cycle near-infrared (NIR) and extreme ultraviolet (XUV) attosecond pulses. The UV light is obtained via third-harmonic generation in argon or neon gas when focusing a phase-stabilized NIR driving field inside a glass cell that was designed to support high pressures for enhanced conversion efficiency. A recirculation system allows reducing the large gas consumption required for the nonlinear process. Isolated attosecond pulses are generated using the polarization gating technique, and the photon spectrometer employed to characterize the XUV radiation consists of a new design based on the combination of a spherical varied-line-space grating and a cylindrical mirror. This design allows for compactness while providing a long entrance arm for integrating different experimental chambers. The entire interferometer is built under vacuum to prevent both absorption of the XUV light and dispersion of the UV pulses, and it is actively stabilized to ensure an attosecond delay stability during experiments. This table-top source has been realized with the aim of investigating UV-induced electron dynamics in neutral states of bio-relevant molecules, but it also offers the possibility to implement a manifold of novel time-resolved experiments based on photo-ionization/excitation of gaseous and liquid targets by ultraviolet radiation. UV pump–XUV probe measurements in ethyl-iodide showcase the capabilities of the attosecond beamline.

## I. INTRODUCTION

The advent of attosecond (1 as = $10^{-18}$ s) light sources based on high-order harmonic generation (HHG)[1,2] represented a breakthrough for ultrafast laser spectroscopy and paved the way for the investigation of electron dynamics in matter.[3] In HHG, focusing an intense femtosecond (fs) laser pulse onto a gas target enables an electron to escape the atomic potential, gain substantial ponderomotive energy, and recombine with the parent ion within a single cycle of the driving electric field. The recombination produces an

12 September 2024 12:04:06

attosecond light pulse in the extreme ultraviolet (XUV) or soft x-ray spectral domains, offering the shortest probe pulse to date. Typically, attosecond pulses are combined with near-infrared (NIR) pulses in a pump–probe configuration for time-resolved measurements, and attosecond beamlines are specifically designed for experiments in the gas phase,[4–11] aqueous solutions,[12] or with a particular interest for the solid state.[13–20] In fact, the realization of XUV-pump XUV-probe schemes,[21,22] although allowing for the highest temporal resolution, still presents several technological challenges mostly due to the limited photon flux of the XUV light sources.

When HHG is driven by few-cycle 800 nm pulses, the available photon energies for an experiment usually span in the 15–100 eV range and can further be extended depending on the generation parameters. Because these photon energies are above the ionization potential of most molecules, the use of attosecond XUV pump pulses inevitably leads to the ionization of the system under study. However, many processes playing key roles in biology and chemistry are triggered by photoexcitation of neutral molecules, especially in the ultraviolet (UV) spectral region between 190 and 350 nm. For instance, the absorption of UV photons in nucleic acid bases can initiate molecular dynamics occurring on timescales from few-femtosecond to several nanoseconds.[23–25] Since the electron dynamics that evolve on a much faster timescale can play a major role in UV-induced photochemistry, a promising probing scheme should combine attosecond XUV probe pulses with few-fs and ultrabroadband ultraviolet pump pulses.[26–28]

In this article, we present a beamline for STeering Attosecond electRon dynamics in biomolecules with UV–XUV LIGHT pulses (STARLIGHT). It combines isolated attosecond pulses (IAPs) and the previously reported few-femtosecond UV pulses,[29] aiming at time-resolved experiments based on the photoexcitation of molecular targets by ultraviolet radiation with an unprecedented temporal resolution. Alternatively, also few-optical-cycle NIR pulses can also be combined with the attosecond XUV or the few-fs UV pulses, allowing for a remarkable flexibility of possible pump–probe schemes. The beamline is intended to be used for studying UV-induced electron dynamics in neutral bio-relevant molecules probed by XUV ionization. These experiments will follow recent investigations of molecular dynamics in amino acids and nucleobases that provided insights into the charge migration process and the ultrafast photo-fragmentation dynamics.[30–34] An overview of the beamline is presented in Sec. II followed by a description of the UV pulse generation setup in Sec. III. Section IV describes the generation and characterization of the isolated attosecond pulses as well as a new design of a compact XUV photon spectrometer. Section V reports the passive and active stabilization of the beamline required to reach an attosecond delay stability. Section VI provides an example of an application using the UV pump–XUV probe scheme for time-resolved mass spectrometry.

## II. BEAMLINE OVERVIEW

The beamline is seeded with 1.25-mJ, 1-kHz, 5-fs NIR pulses, obtained by hollow-core-fiber compression[35] of a titanium:sapphire laser (Femtopower, SpectraPhysics). In addition, the carrier–envelope phase (CEP) of the laser pulses is actively stabilized, as a main ingredient to generate isolated attosecond pulses, as shown in Sec. IV. Figure 1 depicts the optical setup of the beamline.

In chamber 1, the seeding pulses are split by a 1-mm thin beamsplitter to create the pump–probe arms. 70% of the incoming beam is reflected by the beamsplitter (path A) and used for HHG, as shown in Sec. IV B. In this arm, isolated attosecond pulses are obtained by using the polarization gating (PG) technique,[36] while the residual NIR light co-propagating with the attosecond pulses is filtered out using metallic filters. The light transmitted by the beamsplitter (30% of the seeding energy) is sent onto a flat metallic mirror (M in chamber 1) that is mounted on a closed-loop linear positioner. By translating M, two arms can be alternatively seeded, i.e., path B or path C. In path B, the few-cycle NIR pulses are recombined with the XUV pulses in chamber 3 through a 3.5-mm diameter drilled mirror, and both arms are focused into the interaction region by a $150 \times 20 \times 15$ mm$^3$ gold-coated toroidal mirror (TM) that is mounted in chamber 4. This XUV–NIR scheme allows, for example, the attosecond pulses to be characterized by using the attosecond streak camera method.[37,38]

In path C, instead, the NIR pulses are exploited for the generation of few-cycle UV pulses, as shown in Sec. III. The broadband UV pulses are produced in gas via third-harmonic generation (THG, chamber 6) and separated from the residual NIR in chamber 5 using a superpolished silicon mirror at Brewster angle. With this approach, ~40% of the UV radiation is preserved while the NIR is attenuated by more than three orders of magnitude. In this chamber, a mirror placed on a linear positioner can be used to extract the UV beam for spectral and power measurements.

The beam is recombined with the XUV line in chamber 4 by using a narrow-angle noncollinear geometry (<1°). A mirror mounted on a linear positioner before the exit of chamber 4 can be used to extract the beams. This allows the foci at the interaction region to be imaged and the beams to be spatially and temporally overlapped by using a CCD camera. Wedge pairs are placed in both paths B and C to control the dispersion and the carrier-envelope phase. Delay lines are also integrated to synchronize the pump–probe interferometer arms. The pump–probe delay is controlled with attosecond precision by using piezo-based linear positioners (PiezoSystem Jena). An XUV photon spectrometer is placed behind the interaction region to monitor the spectral properties of the XUV radiation while running experiments, as shown in Sec. IV A.

## III. GENERATION OF FEW-FEMTOSECOND UV PULSES

### A. Third-harmonic generation in gas

After the first demonstration of second harmonic generation (SHG) employing laser pulses,[39] THG has been deeply investigated as a next step toward developing nonlinear optics and producing ultraviolet radiation. In crystals, cascaded schemes starting with SHG followed by sum frequency generation are generally employed rather than direct THG due to the increased conversion efficiencies, up to 80%, provided by birefringent phase-matching.[40–42] Using gases as nonlinear media, other techniques, such as spectral broadening via self-phase modulation or cross-phase modulation in gas-filled hollow–core fibers,[43,44] four-wave mixing through filamentation,[45,46] or direct frequency tripling,[29,47–49] have also been demonstrated. Self-compressed and spectrally tunable ultraviolet pulses were also recently reported, exploiting resonant dispersive wave (RDW) emission[50–52] or four-wave mixing[53] in hollow-
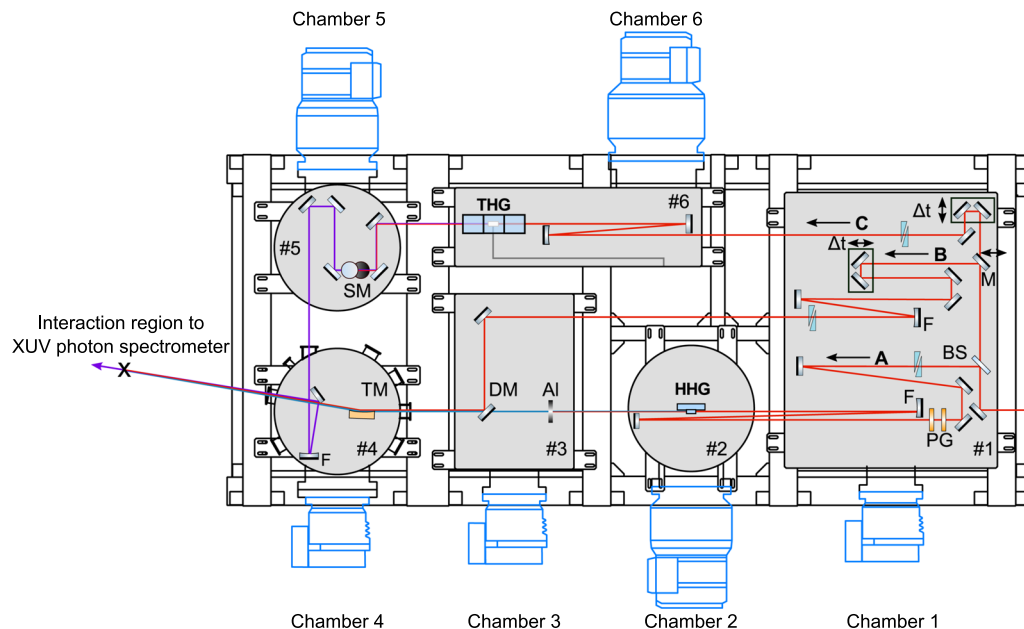
**FIG. 1.** Top view of the beamline. The NIR beam is divided in chamber 1 using a beamsplitter (BS). The reflected beam in path A undergoes a polarization gating (PG) for high-harmonic generation (HHG). The transmitted NIR can either be used as is via path B or sent into path C for third-harmonic generation (THG) by adding or removing a mirror placed on a motorized stage (M). A pulsed valved is used in chamber 2 where the NIR beam is focused for HHG. Chamber 3 is used to recombine paths A and B using a drilled mirror (DM). THG occurs in chamber 6, and the ultraviolet light is separated from the fundamental field in chamber 5 using a silicon mirror (SM) at Brewster angle. In this chamber, the UV light can be extracted for characterization (energy and spectrum). All paths merge in chamber 4 where the XUV and NIR beams are focused into the interaction region by a toroidal mirror (TM). To ensure a spatial overlap at the interaction region along the light propagation axis, a curved mirror (F) in path B is used to create an intermediate focus for which the distance to TM matches the distance between the HHG focus position and TM in path A. The UV beam is focused using an aluminum mirror and sent into the interaction region in a noncollinear geometry. A mirror placed just before the output of the chamber (not shown) can be translated to extract the beams for spatial imaging. The entire interferometer is actively stabilized for attosecond delay stability. Adapted with permission from V. Wanie, "Probing and controlling few-femtosecond dynamics with ultrashort laser pulses: from gases to solids," Ph.D. dissertation (Université du Quebec, 2020).

capillary fibers. The choice of nonlinear media depends on the desired pulse energy and duration. The large bandwidth required to support few-femtosecond UV pulses prevents the use of nonlinear crystals due to limited phase-matching bandwidths and the strong dispersion they impart to the pulse along propagation. For this reason, gas-based UV generation methods are typically favorable to produce ultrabroad bandwidths due to their quasi-dispersion-free properties, however, at the cost of providing lower conversion efficiencies.

Figure 2 shows a glass cell that has been designed to support high gas pressures. It allows us to reach an increased density of emitters in order to compensate for the lower conversion efficiency of gases. Starting from a $20 \times 5$ mm$^2$ fused-silica slab, a portion is reduced to 3-mm width (top half in Fig. 2(a)). The reduced portion contains a 3-mm long channel for laser propagation, micro-machined using Femtosecond Laser Irradiation followed by Chemical Etching (FLICE).[54] On the upper large surface parallel to this channel, a hole is made to hold a 3-mm diameter metallic tube with Swagelok fittings used for injecting the gas. The central cell consists of a 3-mm long cylindrical channel with a progressively reduced diameter from 600 $\mu$m down to 400 $\mu$m at the extremities to confine the gas in a restricted volume during THG and limit the outflow. The cell is integrated into a differential pumping system, as shown in Sec. III B, making the THG setup compatible with a high-vacuum environment.

Figure 3 shows a comparison of UV generation performances between argon and neon gases when focusing the 5-fs NIR pulses into the glass cell. Using a driving intensity of $4.6 \times 10^{14}$ W cm$^{-2}$, a broad spectrum is achieved with 1 bar of argon (purple line), resulting in a 1.9 fs Fourier transform limit (TL) duration. A pulse
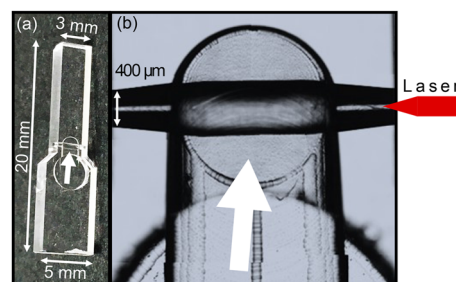


**FIG. 2.** (a) Image of the $20 \times 5$ mm$^2$ fused silica cell used for THG. The white arrow indicates the gas flow direction. (b) Enlarged view of the coupling region. The laser is focused into a 400 $\mu$m aperture and propagates along a 3-mm gas-filled channel micro-machined using the FLICE technique. Reproduced with permission from V. Wanie, "Probing and controlling few-femtosecond dynamics with ultrashort laser pulses: from gases to solids," Ph.D. dissertation (Université du Quebec, 2020).

**FIG. 3.** UV spectra generated in 1 bar of Ar (purple line) and 10 bars of Ne (orange line) using the same NIR pulse intensity, respectively, supporting TL of 1.9 and 2.1 fs. The green line indicates the spectrum corresponding to the highest pulse energy obtained in neon by tuning the UV generation parameters, resulting in a 1.9 fs TL duration.



**FIG. 4.** Differential pumping setup and gas recirculation system. A manual valve (1) allows us to control with precision the gas flow injected into the THG cell residing in the central part of a differential pumping arrangement made of three sub-chambers. A roots pump (2) collects the residual gas coming from the central subunit while a second one (3) collects the remaining gas flowing into the later sub-chambers. The latter pump is also used for backing the turbomolecular pump of the main chamber where a $10^{-4}$ mbar vacuum level can be preserved when using argon. A diaphragm pump (4) is next used for compression and the gas is stocked into a 2-l tank (5). The compressed gas from the tank can be sent back into the THG cell using the manual valve (1). A number of valves and pressure gauges are used to operate and monitor the system performances. Reproduced with permission from V. Wanie, "Probing and controlling few-femtosecond dynamics with ultrashort laser pulses: from gases to solids," Ph.D. dissertation (Université du Quebec, 2020).
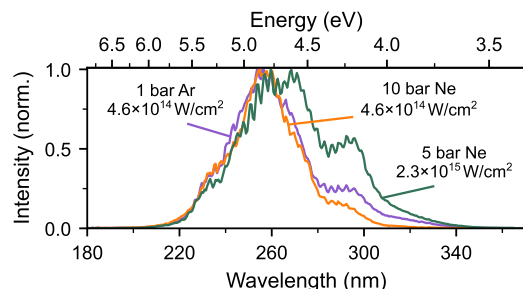
energy of 150 nJ at the generation point was measured by using an optometer (Gigahertz-Optik: ISD-5P–SiUV) and considering the propagation loss of our optical setup. Increasing the NIR intensity or gas pressure results in a lower conversion efficiency due to the ionization of the target. This can be circumvented by using neon with a larger ionization potential (21.6 eV). In this case, we can increase the pressure as high as 10 bars with the same driving NIR intensity (orange line). A slightly narrower spectrum is obtained with a TL of 2.1 fs (orange line), however, with a higher pulse energy of 175 nJ. By optimizing the generation parameters, 260 nJ/pulse for a TL of 1.9 fs was obtained using 5 bar of neon and an NIR intensity of $2.3 \times 10^{15}$ W cm$^{-2}$ (green line). Moreover, we recently achieved pulse energies up to 0.8 $\mu$J by integrating the entire differential-pumping scheme described in Sec. III B within the microfluidic glass chip, leading to both higher gas confinement for THG and better residual gas extraction efficiency.[55] This new design will be incorporated into our attosecond beamline in the near future.

## B. Differential pumping and recirculation system

In order to ensure high vacuum in chamber 6, the glass cell is placed into a differential pumping system made of three sub-chambers, as shown in Fig. 4. The cell is mounted in the central section, and the gas for THG is evacuated toward the lateral sub-chambers through 0.8-mm diameter apertures. The apertures are realized on thin plates that can be easily mounted at the interface between the lateral sub-chambers and the central section. Similar plates are also mounted at the interface between the lateral sub-chambers and the main vacuum chamber. Furthermore, the central section is connected to the wall of chamber 6 through a bellow and pumped by a roots pump (55 m$^3$/h) that collects most of the outflowing gas. In a similar manner, the lateral sub-chambers are evacuated by a second roots pump that is also used as a backing pump for the turbomolecular pump of chamber 6. To further improve the overall vacuum in the beamline, small-diameter apertures are also fixed at the interface between chamber 6 and chamber 1 and between chamber 6 and chamber 5, as supplementary differential pumping elements. Although the gas load is spatially confined by the above-mentioned scheme, the local gas consumption is extremely high (2 bar L/min), making the entire setup hardly sustainable and potentially really expensive. To overcome this limitation, the THG setup
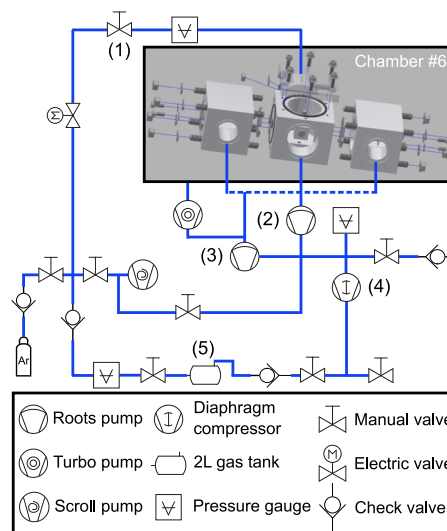
has been equipped with a gas recirculation circuit, also shown in Fig. 4.

The exhausts of the roots pumps are connected to a diaphragm pump via 6-mm Swagelok connections. The gas collected from the pumps exhausts is compressed into a 2-l tank to a pressure of up to 7 bars. Check valves are placed upstream and downstream of the tank to guarantee the right flow direction. The compressed gas is then sent back to the UV generation cell. In order to test the performances of the recirculation system, the argon pressure was measured with a residual gas analyzer (RGA) placed in chamber 5 and monitored as a function of time. The gas bottle was closed so that the filled tank was the only supply source. The result is shown by the blue curve in Fig. 5.

Over the 3-h measurement, 96% of the initial gas pressure is preserved. The pressure measured at the tank (3 bars) and at the roots pump exhausts (0.52 bar) remained constant over the entire period. We note that no degradation in the ultraviolet spectrum nor pulse energy is observed down to this level of purity. The excellent efficiency of the system would allow an operation over 37 h with a consumption of only 1 l of gas in the tank. Without recirculation, instead, the same gas consumption (1 l) is reached after 1.5 min, with a consumption rate of 2 bar l/min. For comparison, a similar measurement was done by including in the recirculation system only the sub-chambers of the THG setup, i.e., excluding the residual gas
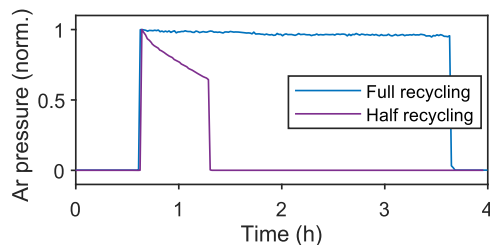
**FIG. 5.** Argon recirculation performances. After 3 h (blue curve), 96% of the initial argon pressure is detected by a residual gas analyzer when the full recycling scheme is employed. When the gas collected from the turbomolecular pump of chamber 6 is not recycled (half recycling, purple curve), the efficiency goes down to 66% in 40 min. Adapted with permission from V. Wanie, "Probing and controlling few-femtosecond dynamics with ultrashort laser pulses: from gases to solids," Ph.D. dissertation (Université du Quebec, 2020).



**FIG. 6.** High-harmonic generation in krypton with $\sim 800~\mu$J, 5-fs pulses at 800 nm. (a) Raw image showing the spatial profile of the harmonics. (b) Corresponding spatially integrated signal with the calibrated axis. Harmonics 11–21 are observed. Reproduced with permission from V. Wanie, "Probing and controlling few-femtosecond dynamics with ultrashort laser pulses: from gases to solids," Ph.D. dissertation (Université du Quebec, 2020).

pumped out by the turbomolecular pump of chamber 6. The result is reported in Fig. 5 (purple curve). This "half recycling" scheme shows larger losses, with the initial argon pressure reduced to 66% after only 40 min. During this period of time, the tank pressure dropped from 3.1 to 1.5 bars and the exhaust pressure dropped from 0.52 to 0.34 bars. However, although requiring a continuous refill of the tank, the gas consumption in the "half recycling" scheme is still significantly reduced compared to not using any recirculation system at all.

## IV. XUV GENERATION AND DETECTION

The NIR laser pulses propagating along path A (see Fig. 1) are focused by a $f = -700$ mm silver mirror into a 6-mm channel filled with gas for HHG. The gas target is delivered into the interaction by a water-cooled pulsed valve (Attotech), which is triggered at 1 kHz repetition rate and synchronized with the laser. The opening time of the valve is typically adjusted from 120 to 150 $\mu$s with a backing pressure between 1 and 2 bars. Argon, krypton, and xenon are alternatively used for HHG, depending on the desired XUV spectral range. To optimize the alignment of the laser through the gas target, the valve is mounted on a structure with four motorized positioners, consisting of three translations and one rotation (Physik Instruments). Figure 6 shows a typical XUV spectrum generated in krypton and measured with a customized photon spectrometer described in Sec. IV A.

### A. XUV photon spectrometer

We report here an innovative design of an XUV spectrometer for the spectral characterization of HHG pulses in the 15–50 eV range. In a prototypical spectrometer, the incoming light is spectrally dispersed by a grating and imaged in the Fourier space on a photodetector. The higher the groove density of the grating, the higher the spectral resolution of the spectrometer. In order to further increase the spectral resolution of the instrument, an entrance slit is usually employed to spatially confine the light source to be imaged. Although narrow slit apertures allow for high spectral resolution, they also limit the amount of photons reaching the detector.
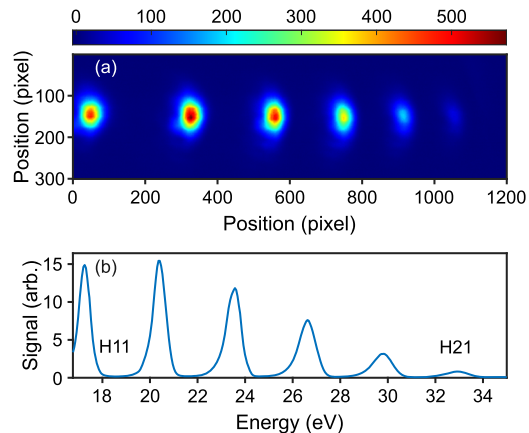
Common spectrometers for XUV light consist of a grazing-incidence mirror focusing the light source onto a slit placed at a fixed distance from a spherical varied-line-space (SVLS) grating. The SVLS provides the so-called "flat-field" property, where all the spectral components are focused onto the same plane rather than on a cylindrical surface as for equal line-space gratings.[56] This allows the acquisition of XUV spectra using a two-dimensional detector.

Usually, the XUV light generated by HHG is refocused by a grazing-incidence toroidal mirror onto the target under study, i.e., into the interaction point where experiments occur. If the toroidal mirror works with a 1:1 refocusing magnification factor, the XUV focus at the interaction point presents minimal aberrations, allowing it to be directly used as the source point for the spectrometer. This configuration shows several advantages. First, the XUV spectrometer can be mounted directly behind the experimental chamber for simultaneous diagnostics. Second, the small size and quality of the XUV focus make the use of an entrance slit unnecessary, which maximizes the photon flux entering the spectrometer.[57]

In our beamline, a 1-m focal-length toroidal mirror is used to refocus the HHG light source into the interaction point for experiments. Such a long focusing arm is chosen to be compatible with large-footprint experimental setups. However, the entrance arm of the XUV spectrometer (specified by the grating) is much shorter, i.e., only 350 mm. As a common solution to overcome this limitation and realize a long entrance-arm spectrometer, a second toroidal mirror that is a replica of the first one can be mounted behind the experimental chamber. It collects the XUV light from the interaction region and refocuses it, again with a 1:1 magnification factor, into the source point of the grating. This configuration usually requires that the second toroidal mirror and the grating are mounted in separate vacuum chambers, significantly increasing the overall footprint of the XUV spectrometer. As an alternative solution, a retractable spherical mirror can be placed before the first toroidal mirror, i.e.,

the one that focuses the XUV light into the experimental chamber. This spherical mirror can either be used to steer the beam toward an XUV spectrometer, or it can be retracted for the beam to reach the toroidal and the experimental interaction point.[15] The main disadvantage of this method is that the XUV spectrum cannot be monitored while running experiments.

In order to improve the compactness of our XUV spectrometer while keeping a long entrance arm, we combined an SVLS grating (Hitachi) with a convex (divergent) cylindrical mirror at a grazing incidence angle (Fig. 7). The gold-coated grating has a 5649 mm radius of curvature, a blaze angle of 3.7°, and a central groove density of 600 lines/mm. The gold-coated cylindrical mirror is used to create a virtual image of the XUV focus at the source point of the grating while keeping a relatively long entrance arm of 750 mm. Then, the grating provides a flat spectral plane at a distance of 469 mm, where the detector is mounted. The detector consists of a 40-mm-diameter microchannel plate (MCP) and a P43 phosphor screen (Photek), and it is placed on a translation stage to span the spectral plane. Typically, a translation of 10 mm is sufficient to acquire a spectrum spanning from 15 to 50 eV in two images. Since the cylindrical mirror does not focus along the sagittal (vertical) plane, the spatial profile of the harmonics can also be monitored along the vertical axis and used to measure the XUV divergence. The images produced by the phosphor screen are recorded by a CMOS camera (Hamamatsu). To further reduce the footprint of the instrument, a $50 \times 50$ mm$^2$ silver mirror is mounted at 45°, enabling the image to be recorded perpendicularly to the MCP detector, i.e., by mounting the CMOS camera vertically. The total length of the spectrometer is about 80 cm.

## B. Generation of isolated attosecond pulses

Isolated attosecond pulses (IAPs) are obtained using the polarization gating (PG) technique. In this method, a combination of two birefringent glass plates, i.e., a retarder plate and a $\lambda/4$ plate, is used to reshape the polarization of the driving electric field.[36] The resulting pulses show a narrow gate of linear polarization across the envelope peak while being circularly polarized on the rising and the trailing edges. Since HHG is efficient only for a linearly polarized driving field,[58] attosecond pulses are generated only within the linear polarization gate. If the gate is narrower than a driving optical cycle and the CEP ($\Psi$) is equal to $k * \pi/2$ (with $k = 1, 3, 5, \ldots$), an IAP is produced through PG.
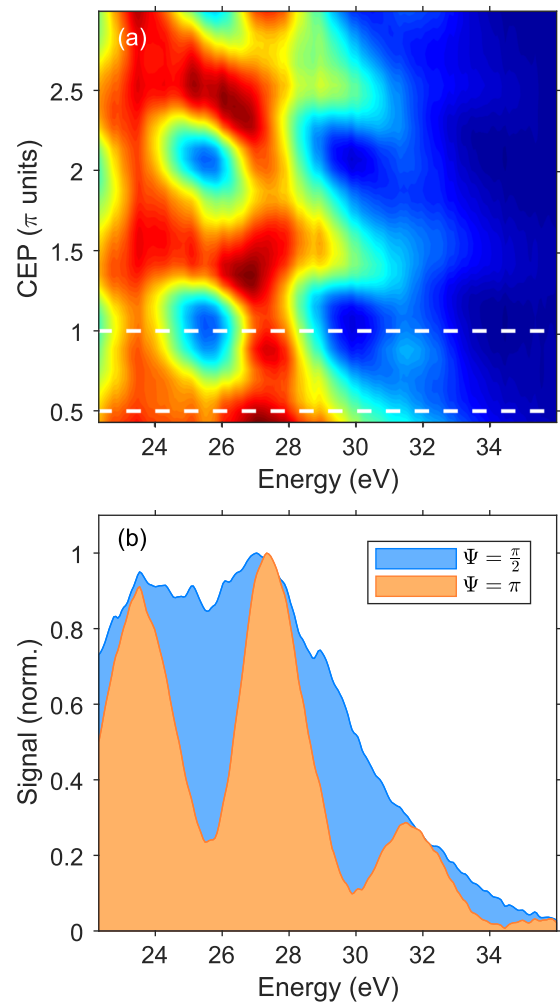


FIG. 8. (a) XUV spectrum of HHG in krypton as a function of the carrier–envelope phase of the NIR driving field when the polarization gating technique is applied. Each $\pi/2$ dephasing of the CEP transforms the continuous spectrum characteristic of an isolated pulse into a harmonic comb and vice versa. (b) Spectral cuts for CEP values $\Psi = \frac{\pi}{2}$ and $\pi$, corresponding to the horizontal dashed lines displayed in (a). Reproduced with permission from V. Wanie, "Probing and controlling few-femtosecond dynamics with ultrashort laser pulses: from gases to solids," Ph.D. dissertation (Université du Quebec, 2020).
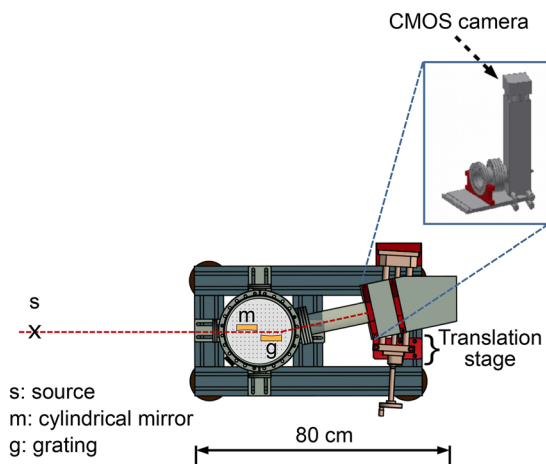


FIG. 7. Scheme of the XUV photon spectrometer (top view). 75 cm away from the source, a cylindrical mirror in combination with a spherical grating images the XUV radiation onto a microchannel plate (MCP) amplifier followed by a phosphor screen. The image is collected by a mirror placed at 45° and sent to a CMOS camera. Due to the restricted area of the MCP, the detector is translated along the spectral axis to acquire the full spectrum. The length of the spectrometer is about 80 cm. Reproduced with permission from V. Wanie, "Probing and controlling few-femtosecond dynamics with ultrashort laser pulses: from gases to solids," Ph.D. dissertation (Université du Quebec, 2020).

In the case of the 5-fs NIR pulses used to seed the beamline, the above-mentioned conditions are obtained by combining a 193 $\mu$m-thick quartz retarder plate and an air-spaced, broadband $\lambda/4$ waveplate (B-Halle). Figure 8 shows the XUV spectra obtained by HHG in krypton as a function of the CEP of the driving pulse. The CEP was controlled by a motorized glass wedge translated in a direction perpendicular to the laser propagation axis. For $\Psi = \pi/2$ and $3\pi/2$, continuous XUV spectra are generated [see Fig. 8(b), blue curve], corresponding to an IAP. Instead, for $\Psi = \pi$ and $2\pi$, the condition to produce an IAP is expected to be lost, and the XUV spectrum is strongly modulated [see Fig. 8(b), orange curve], corresponding to a train composed of mainly two pulses. This configuration provides XUV IAPs with a duration of 300 as[30] and 100 pJ energy per pulse. The pulse energy can reach the nanojoule range if the ionization gating approach is employed[30,59] instead of the polarization gating, and the intensity is estimated to be between $10^8$ and $10^9$ W/cm$^2$ depending on the gating method.[36,59]

## V. PUMP–PROBE DELAY STABILIZATION

To ensure an attosecond delay stability during experiments, the relative path between the pump and the probe arms must be kept constant within a few nanometers. In this context, sources of high- and low-frequency noise, such as vibrations from the vacuum pumps and temperature-driven effects, must be identified, and the effect on the delay must be compensated by exploiting both passive and active stabilization schemes. In long (several meters) interferometers, the effect of such noise sources, especially low-frequency drifts, may be particularly harmful.

The interferometer arms of our beamline are about 5.75 m long. To passively stabilize the beamline, all vacuum chambers are mounted on an external frame made of aluminum profiles. The frame is decoupled from the optical table and carries vibrations from the turbomolecular pumps to the floor. The structure is also used to support gas panels, electronic control units, and cables that are necessary to operate the beamline while being potential sources of noise. Inside the chambers, the breadboards on which the optical components stand are connected to a single optical table (TMC) using internal posts. Each post is vacuum-sealed by a surrounding CF40 bellow to damp any residual vibrations coming from the chambers. The flat surface at the bottom extremity of the bellow is welded to the post on the vacuum side, while the air side is used for clamping on the optical table.

The active stabilization is obtained by using a continuous wave (CW) laser that co-propagates with the main laser along the pump–probe interferometer. Since the silicon mirror mounted in path C (see Sec. II) strongly reduces any NIR spectral components, a standard 633 nm helium–neon laser is not a suitable option to be used as a CW stabilization laser. Therefore, a frequency-stabilized diode laser with a wavelength of 473 nm (Hübner Photonics) was employed.[8] At the end of the interferometer, the CW laser is extracted, and the interference pattern produced by the two recombined paths is recorded on a CCD camera operating at 12.5 Hz. A narrow-bandpass interference filter centered at 470 nm (Thorlabs) is used to filter out the co-propagating NIR light. In order to set the active stabilization, the interference pattern is Fourier transformed, and the main spatial frequency component is extracted together with the correspondent phase. Since any spatial jitter or
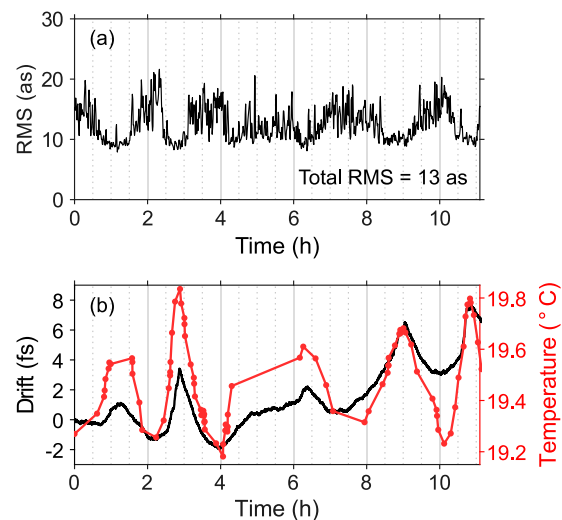
**FIG. 9.** Beamline stability measurement over 11 h. (a) Calculated in-loop RMS of the phase error using a moving window containing 1000 points (1.4 min). The RMS over the entire measurement is 51 mrad, corresponding to a delay stability of 13 as. (b) Comparison between the corrected drift (black curve) over the acquisition time and the room temperature variation (red curve). Reproduced with permission from V. Wanie, "Probing and controlling few-femtosecond dynamics with ultrashort laser pulses: from gases to solids," Ph.D. dissertation (Université du Quebec, 2020).

drift in the pump–probe interferometer is directly imprinted in the value of the above-mentioned phase, the active stabilization aims to keep the phase constant with the lowest deviation. To do this, a proportional–integral (PI)-based feedback loop is used to act on a piezoelectric positioner, with the purpose of compensating for any phase variation.[60] We note that the same positioner is used to set the pump–probe delay during experiments.

Figure 9 reports the stability of the beamline during 11 hours of active stabilization. Shown in Fig. 9(a) is the moving root mean square (RMS) of the phase error over the entire scan, employing a sliding window containing 1000 data points (1.4 minutes). For each translation of the window, the previous 500 points are conserved. An in-loop RMS of 51 mrad on the phase error is obtained over the full measurement, corresponding to a 13 as delay stability. Moreover, we investigated the main sources of slow drifts in the interferometric delay. In this context, Fig. 9(b) shows a clear correlation between the room temperature (red dotted curve) and the drift corrected by the active stabilization over 11 h (black solid line). In particular, it is evident that already small temperature variations of about 0.6 °C reflect into delay drifts of several femtoseconds.

## VI. UV PUMP–XUV PROBE MEASUREMENTS

In addition to Sec. III, the properties of the UV pulses delivered by the setup and a first demonstration of few-fs UV pump–NIR probe measurements have also been discussed in previous studies.[29,61] Here, we briefly report on the capabilities of the beamline for UV pump–XUV probe experiments.

The UV and XUV pulses are focused in the center of a reflectron type time-of-flight mass spectrometer using the noncollinear

geometry described in Sec. II. Ethyl-iodide ($C_2H_5I$ 98%, Sigma-Aldrich) has been injected through a skimmer in the interaction region by producing vapor at room temperature, resulting in a pressure in the interaction chamber of $5.3 \times 10^{-6}$ mbar. Ethyl-iodide was chosen as a benchmark sample since alkyl iodides possess high cross sections in the deep ultraviolet and have been widely investigated.[62–65] Figure 10(a) reports the spectrum of the UV pulses (left) and XUV pulses (right) used in the experiment. The UV radiation was centered at a photon energy of 4.5 eV, with a TL of 2.2 fs and a pulse energy of 50 nJ. The XUV radiation was generated in krypton, as reported in Sec. IV, and covers the energy region between 17 and 43 eV. Figure 10 (b-c) shows the measured ion yields as a function of the UV–XUV time delay for the selected fragmentation

products $C_2H_2^+$ (b) and $C_2H_5^+$ (c). For both fragments, the contrast of the ion yield between negative and positive delays is in the order of 2%. The curves were fitted using an exponentially modified Gaussian distribution, resulting in a standard deviation ($\sigma$) of $5.88 \pm 1.22$ fs for the $C_2H_2^+$ fragment and $5.90 \pm 1.14$ fs for the $C_2H_5^+$ fragment. We note that we also extract a relative delay of $6.72 \pm 0.93$ fs between the two fragments, which is a signature of the ultrafast molecular dynamics captured in our measurement. A more detailed interpretation of the UV-induced fragmentation dynamics of ethyl-iodide will be described in a forthcoming publication.

With a clear signature of a time-dependent interaction between the UV and XUV pulses, these measurements demonstrate the feasibility of UV pump–XUV probe experiments using our attosecond beamline.

## VII. SUMMARY

We presented here a novel pump–probe beamline combining XUV-isolated attosecond pulses, few-femtosecond UV pulses, and few-cycle NIR pulses. We showed that the beamline is suitable for a new class of UV-based experiments. Furthermore, the innovative gas recirculation system that was developed allows for the realization of high-statistics, long-acquisition-time experiments, in which the gas consumption for the UV generation is minimized and kept sustainable. This method is likely to be extremely beneficial for other purposes, such as the operation of gas-filled hollow–core fibers or the generation of XUV and soft x-rays through HHG, for which high gas pressures are required *in situ*.[66,67] A stricter control of the gas purity will be required to preserve the conversion efficiency of the latter highly nonlinear process. A new design of a compact XUV spectrometer was also described, based on the combination of an SLVS grating and a cylindrical mirror. While keeping an extremely compact footprint, it provides a long entrance arm that is suitable for the installation of large detection systems and sample sources such as two-sided spectrometers.[68] These will particularly benefit the investigation of large molecular systems, allowing for covariance measurements that can be used to access simultaneously nuclear and electronic degrees of freedom.[69] The STARLIGHT beamline provides a unique setup for the future investigation of UV-induced electron dynamics in biochemically relevant molecules with temporal resolution from a few femtoseconds down to a few hundred attoseconds.[61]



**FIG. 10.** Time-resolved measurements in ethyl-iodide using the UV and XUV spectra shown in (a), normalized individually. The beamline was driven by near-infrared pulses with 4.8 fs duration. The temporal evolution of the ion yields is shown for fragment ions $C_2H_2^+$ with 26 u (b) and $C_2H_5^+$ with 29 u (c) as blue-dotted lines. For each delay, the signal was normalized by the total ion yield. Each curve was fitted using an exponentially modified Gaussian distribution (red lines).

## AUTHOR DECLARATIONS

### Conflict of Interest

The authors have no conflicts to disclose.

### Author Contributions

V.W. and S.R contributed equally to this work.

**V. Wanie**: Formal analysis (lead); Investigation (lead); Visualization (lead); Writing – original draft (lead); Writing – review & editing (lead). **S. Ryabchuk**: Formal analysis (equal); Investigation (equal); Visualization (equal); Writing – review & editing (equal). **L. Colaizzi**: Investigation (supporting); Writing – review & editing (equal). **M. Galli**: Investigation (supporting); Writing – review & editing (supporting). **E. P. Månsson**: Formal analysis (supporting); Investigation (supporting); Software (lead); Visualization (supporting); Writing – review & editing (equal). **A. Trabattoni**: Investigation (supporting); Writing – original draft (supporting); Writing – review & editing (equal). **A. B. Wahid**: Investigation (supporting). **J. Hahne**: Investigation (supporting). **A. Cartella**: Investigation (supporting); Writing – review & editing (equal). **K. Saraswathula**: Investigation (supporting). **F. Frassetto**: Conceptualization (equal); Investigation (supporting); Writing – review & editing (equal). **D.P. Lopes**: Investigation (supporting). **R. Martínez Vázquez**: Conceptualization (supporting); Investigation (supporting); Supervision (supporting); Writing – review & editing (equal). **R. Osellame**: Conceptualization (supporting); Resources (supporting); Supervision (supporting); Writing – review & editing (equal). **L. Poletto**: Conceptualization (equal); Investigation (supporting); Resources (supporting); Writing – review & editing (equal). **F. Légaré**: Resources (supporting); Supervision (supporting); Writing – review & editing (equal). **M. Nisoli**: Resources (supporting); Supervision (supporting); Writing – review & editing (equal). **F. Calegari**: Conceptualization (lead); Funding acquisition (lead); Investigation (supporting); Resources (lead); Supervision (lead); Writing – review & editing (equal).

## DATA AVAILABILITY

The data that support the findings of this study are available from the corresponding author upon reasonable request.

## REFERENCES

[1] P. M. Paul, E. S. Toma, P. Breger, G. Mullot, F. Auge, P. Balcou, H. G. Muller, and P. Agostini, "Observation of a train of attosecond pulses from high harmonic generation," Science **292**, 1689–1692 (2001).

[2] M. Hentschel, R. Kienberger, C. Spielmann, G. A. Reider, N. Milosevic, T. Brabec, P. Corkum, U. Heinzmann, M. Drescher, and F. Krausz, "Attosecond metrology," Nature **414**, 509–513 (2001).

[3] R. Borrego-Varillas, M. Lucchini, and M. Nisoli, "Attosecond spectroscopy for the investigation of ultrafast dynamics in atomic, molecular and solid-state physics," Rep. Prog. Phys. **85**, 066401 (2022).

[4] M. Fiess, M. Schultze, E. Goulielmakis, B. Dennhardt, J. Gagnon, M. Hofstetter, R. Kienberger, and F. Krausz, "Versatile apparatus for attosecond metrology and spectroscopy," Rev. Sci. Instrum. **81**, 093103 (2010).

[5] F. Frank, C. Arrell, T. Witting, W. A. Okell, J. McKenna, J. S. Robinson, C. A. Haworth, D. Austin, H. Teng, I. A. Walmsley, J. P. Marangos, and J. W. G. Tisch, "Invited review article: Technology for attosecond science," Rev. Sci. Instrum. **83**, 071101 (2012).

[6] P. Rudawski, C. M. Heyl, F. Brizuela, J. Schwenke, A. Persson, E. Mansten, R. Rakowski, L. Rading, F. Campi, B. Kim, P. Johnsson, and A. L'Huillier, "A high-flux high-order harmonic source," Rev. Sci. Instrum. **84**, 073103 (2013).

[7] S. J. Weber, B. Manschwetus, M. Billon, M. Böttcher, M. Bougeard, P. Breger, M. Géléoc, V. Gruson, A. Huetz, N. Lin, Y. J. Picard, T. Ruchon, P. Salières, and B. Carré, "Flexible attosecond beamline for high harmonic spectroscopy and XUV/near-IR pump probe experiments requiring long acquisition times," Rev. Sci. Instrum. **86**, 033108 (2015).

[8] M. Sabbar, S. Heuser, R. Boge, M. Lucchini, L. Gallmann, C. Cirelli, and U. Keller, "Combining attosecond XUV pulses with coincidence spectroscopy," Rev. Sci. Instrum. **85**, 103113 (2014).

[9] P. Ye, T. Csizmadia, L. G. Oldal, H. N. Gopalakrishna, M. Füle, Z. Filus, B. Nagy-illés, Z. Divéki, T. Grósz, M. Dumergue, P. Jójárt, I. Seres, Z. Bengery, V. Zuba, Z. Várallyay, B. Major, F. Frassetto, M. Devetta, G. D. Lucarelli, M. Lucchini, B. Moio, S. Stagira, C. Vozzi, L. Poletto, M. Nisoli, D. Charalambidis, S. Kahaly, A. Zaïr, and K. Varjú, "Attosecond pulse generation at ELI-ALPS 100 kHz repetition rate beamline," J. Phys. B: At., Mol. Opt. Phys. **53**, 154004 (2020).

[10] H. Srinivas, F. Shobeiry, D. Bharti, T. Pfeifer, R. Moshammer, and A. Harth, "High-repetition rate attosecond beamline for multi-particle coincidence experiments," Opt. Express **30**, 13630 (2022).

[11] S. Luo, R. Weissenbilder, H. Laurell, M. Ammitzböll, V. Poulain, D. Busto, L. Neoričić, C. Guo, S. Zhong, D. Kroon, R. J. Squibb, R. Feifel, M. Gisselbrecht, A. L'Huillier, and C. L. Arnold, "Ultra-stable and versatile high-energy resolution setup for attosecond photoelectron spectroscopy," Adv. Phys.: X **8**, 2250105 (2023).

[12] K. S. Zinchenko, F. Ardana-Lamas, V. U. Lanfaloni, T. T. Luu, Y. Pertot, M. Huppert, and H. J. Wörner, "Apparatus for attosecond transient-absorption spectroscopy in the water-window soft-x-ray region," Sci. Rep. **13**, 3059 (2023).

[13] E. Magerl, S. Neppl, A. L. Cavalieri, E. M. Bothschafter, M. Stanislawski, T. Uphues, M. Hofstetter, U. Kleineberg, J. V. Barth, D. Menzel, F. Krausz, R. Ernstorfer, R. Kienberger, and P. Feulner, "A flexible apparatus for attosecond photoelectron spectroscopy of solids and surfaces," Rev. Sci. Instrum. **82**, 063104 (2011).

[14] M. F. Jager, C. Ott, C. J. Kaplan, P. M. Kraus, D. M. Neumark, and S. R. Leone, "Attosecond transient absorption instrumentation for thin film materials: Phase transitions, heat dissipation, signal stabilization, timing correction, and rapid sample rotation," Rev. Sci. Instrum. **89**, 013109 (2018).

[15] R. Locher, M. Lucchini, J. Herrmann, M. Sabbar, M. Weger, A. Ludwig, L. Castiglioni, M. Greif, M. Hengsberger, L. Gallmann, and U. Keller, "Versatile attosecond beamline in a two-foci configuration for simultaneous time-resolved measurements," Rev. Sci. Instrum. **85**, 013113 (2014).

[16] B. Frietsch, R. Carley, K. Döbrich, C. Gahl, M. Teichmann, O. Schwarzkopf, P. Wernet, and M. Weinelt, "A high-order harmonic generation apparatus for time- and angle-resolved photoelectron spectroscopy," Rev. Sci. Instrum. **84**, 075106 (2013).

[17] Y. Liu, J. E. Beetar, M. Hosen, G. Dhakal, C. Sims, F. Kabir, M. B. Etienne, K. Dimitri, S. Regmi, Y. Liu, A. K. Pathak *et al.*, "Extreme ultraviolet time- and angle-resolved photoemission setup with 21.5 meV resolution using high-order harmonic generation from a turn-key Yb:KGW amplifier," Rev. Sci. Instrum. **91**, 013102 (2020).

[18] V. Stooß, M. Hartmann, P. Birk, G. D. Borisova, T. Ding, A. Blättermann, C. Ott, and T. Pfeifer, "XUV-beamline for attosecond transient absorption measurements featuring a broadband common beam-path time-delay unit and *in situ* reference spectrometer for high stability and sensitivity," Rev. Sci. Instrum. **90**, 053108 (2019).

[19] G. D. Lucarelli, B. Moio, G. Inzani, N. Fabris, L. Moscardi, F. Frassetto, L. Poletto, M. Nisoli, and M. Lucchini, "Novel beamline for attosecond transient reflection spectroscopy in a sequential two-foci geometry," Rev. Sci. Instrum. **91**, 053002 (2020).

[20] D. Bresteau, C. Spezzani, O. Tcherbakoff, J. F. Hergott, F. Lepetit, P. D'Oliveira, P. Salières, R. Géneaux, M. Luttmann, I. Vadillo-Torre, J. Lenfant, S. J. Weber, M. Dehlinger, E. Meltchakov, F. Delmotte, C. Bourassin-Bouchet, J. Im, Z. Chen, J. Caillaux, J. Zhang, M. Marsi, L. Barreau, L. Poisson, D. Dowek, M. Fanciulli, O. Heckmann, M. C. Richter, K. Hricovini, M. Sebdaoui, D. Dennetiere, F. Polack, and T. Ruchon, "FAB10: A user-oriented bandwidth-tunable extreme ultraviolet lightsource for investigations of femtosecond to attosecond dynamics in gas and condensed phases," Eur. Phys. J. Spec. Top. **232**, 2011 (2023).

[21] I. Makos, I. Orfanos, A. Nayak, J. Peschel, B. Major, I. Liontos, E. Skantzakis, N. Papadakis, C. Kalpouzos, M. Dumergue, S. Kühn, K. Varju, P. Johnsson, A. L'Huillier, P. Tzallas, and D. Charalambidis, "A 10-gigawatt attosecond source for non-linear XUV optics and XUV- pump-XUV-probe studies," Sci. Rep. **10**, 3759 (2020).

[22] Martin Kretschmar, Science Advances (2024).

[23] C. E. Crespo-Hernanndez, B. Cohen, P. M. Hare, and B. Kohler, "Ultrafast excited-state dynamics in nucleic acids," Chem. Rev. **104**, 1977–2019 (2004).

[24] C. T. Middleton, K. de La Harpe, C. Su, Y. K. Law, C. E. Crespo-Hernández, and B. Kohler, "DNA excited-state dynamics: From single bases to the double helix," Annu. Rev. Phys. Chem. **60**, 217–239 (2009).

[25] R. Improta, F. Santoro, and L. Blancafort, "Quantum mechanical studies on the photophysics and the photochemistry of nucleic acids and nucleobases," Chem. Rev. **116**, 3540–3593 (2016).

[26] V. Wanie, "Probing and controlling few-femtosecond dynamics with ultrashort laser pulses: From gases to solids." Ph D.thesis, ProQuest, 2020.

[27] M. Galli, V. Wanie, E. P. Månsson, A. Trabattoni, F. Légaré, F. Frassetto, L. Poletto, M. Nisoli, and F. Calegari, "A beamline for attosecond UV pump—XUV probe experiments," EPJ Web Conf. **205**, 002017 (2019).

[28] T. Khurelbaatar, A. Gliserin, J. H. Mun, J. Heo, Y. Lee, and D. E. Kim, "Realization of a continuously phase-locked few-cycle deep-UV/XUV pump-probe beamline with attosecond precision for ultrafast spectroscopy," Appl. Sci. **11**, 6840 (2021).

[29] M. Galli, V. Wanie, D. P. Lopes, E. P. Månsson, A. Trabattoni, L. Colaizzi, K. Saraswathula, A. Cartella, F. Frassetto, L. Poletto, F. Légaré, S. Stagira, M. Nisoli, R. Martínez Vázquez, R. Osellame, and F. Calegari, "Generation of deep ultraviolet sub-2-fs pulses," Opt. Lett. **44**, 1308 (2019).

[30] F. Calegari, D. Ayuso, A. Trabattoni, L. Belshaw, S. De Camillis, S. Anumula, F. Frassetto, L. Poletto, A. Palacios, P. Decleva, J. B. Greenwood, F. Martín, and M. Nisoli, "Ultrafast electron dynamics in phenylalanine initiated by attosecond pulses," Science **346**, 336–339 (2014).

[31] E. P. Månsson, S. De Camillis, M. C. Castrovilli, M. Galli, M. Nisoli, F. Calegari, and J. B. Greenwood, "Ultrafast dynamics in the DNA building blocks thymidine and thymine initiated by ionizing radiation," Phys. Chem. Chem. Phys. **19**, 19815–19821 (2017).

[32] E. Perfetto, A. Trabattoni, F. Calegari, M. Nisoli, A. Marini, and G. Stefanucci, "Ultrafast quantum interference in the charge migration of tryptophan," J. Phys. Chem. Lett. **11**, 891–899 (2020).

[33] E. P. Månsson, S. Latini, F. Covito, V. Wanie, M. Galli, E. Perfetto, G. Stefanucci, H. Hübener, U. De Giovannini, M. C. Castrovilli, A. Trabattoni, F. Frassetto, L. Poletto, J. B. Greenwood, F. Légaré, M. Nisoli, A. Rubio, and F. Calegari, "Real-time observation of a correlation-driven sub 3 fs charge migration in ionised adenine," Commun. Chem. **4**, 73 (2021).

[34] E. P. Månsson, S. Latini, F. Covito, V. Wanie, M. Galli, E. Perfetto, G. Stefanucci, U. De Giovannini, M. C. Castrovilli, A. Trabattoni, F. Frassetto, L. Poletto, J. B. Greenwood, F. Légaré, M. Nisoli, A. Rubio, and F. Calegari, "Ultrafast dynamics of adenine following XUV ionization," J. Phys. Photonics **4**, 034003 (2022).

[35] M. Nisoli, S. De Silvestri, and O. Svelto, "Generation of high energy 10 fs pulses by a new pulse compression technique," Appl. Phys. Lett. **68**, 2793–2795 (1996).

[36] I. J. Sola, E. Mével, L. Elouga, E. Constant, V. Strelkov, L. Poletto, P. Villoresi, E. Benedetti, J.-P. Caumes, S. Stagira, C. Vozzi, G. Sansone, and M. Nisoli, "Controlling attosecond electron dynamics by phase-stabilized polarization gating," Nat. Phys. **2**, 319–322 (2006).

[37] J. Itatani, J. Quéré, G. L. Yudin, M. Y. Ivanov, F. Krausz, and P. B. Corkum, "Attosecond streak camera," Phys. Rev. Lett. **88**, 173903 (2002).

[38] R. Kienberger, E. Goulielmakis, M. Uiberacker, A. Baltuska, V. Yakovlev, F. Bammer, A. Scrinzi, T. Westerwalbesloh, U. Kleineberg, U. Heinzmann, M. Drescher, and F. Krausz, "Atomic transient recorder," Nature **427**, 817 (2004).

[39] P. A. Franken, A. E. Hill, C. W. Peters, and G. Weinreich, "Generation of optical harmonics," Phys. Rev. Lett. **7**, 118 (1961).

[40] W. Seka, S. D. Jacobs, J. E. Rizzo, R. Boni, and R. S. Craxton, "Demonstration of high efficiency third harmonic conversion of high power Nd-glass laser radiation," Opt. Commun. **34**, 469–473 (1980).

[41] J. Ringling, G. Korn, J. Squier, O. Kittelmann, and F. Noack, "Tunable femtosecond pulses in the near vacuum ultraviolet generated by frequency conversion of amplified Ti:sapphire laser pulses," Opt. Lett. **18**, 2035 (1993).

[42] S. N. Zhu, Y. Y. Zhu, and N. B. Ming, "Quasi-phase-matched third-harmonic generation in a quasi-periodic optical superlattice," Science **278**, 843–846 (1997).

[43] T. Nagy and P. Simon, "Generation of 200-$\mu$J, sub-25-fs deep-UV pulses using a noble-gas-filled hollow fiber," Opt. Lett. **34**, 2300–2302 (2009).

[44] C. G. Durfee, S. Backus, H. C. Kapteyn, and M. M. Murnane, "Intense 8-fs pulse generation in the deep ultraviolet," Opt. Lett. **24**, 697–699 (1999).

[45] T. Fuji and T. Suzuki, "Generation of sub-two-cycle mid-infrared pulses by four-wave mixing through filamentation in air," Opt. Lett. **32**, 3330 (2007).

[46] T. Fuji, T. Suzuki, E. E. Serebryannikov, and A. Zheltikov, "Experimental and theoretical investigation of a multicolor filament," Phys. Rev. A **80**(6), 063822 (2009).

[47] G. H. C. New and J. F. Ward, "Optical third-harmonic generation in gases," Phys. Rev. Lett. **19**, 556–559 (1967).

[48] U. Graf, M. Fiess, M. Schultze, R. Kienberger, F. Krausz, and E. Goulielmakis, "Intense few-cycle light pulses in the deep ultraviolet," Opt. Express **16**, 18956–18963 (2008).

[49] F. Reiter, U. Graf, M. Schultze, W. Schweinberger, H. Schröder, N. Karpowicz, A. M. Azzeer, R. Kienberger, F. Krausz, and E. Goulielmakis, "Generation of sub-3 fs pulses in the deep ultraviolet," Opt. Lett. **35**, 2248 (2010).

[50] J. C. Travers, T. F. Grigorova, C. Brahms, and F. Belli, "High-energy pulse self-compression and ultraviolet generation through soliton dynamics in hollow capillary fibres," Nat. Photonics **13**, 547–554 (2019).

[51] C. Brahms, T. F. Grigorova, F. Belli, and J. C. Travers, "High-energy ultraviolet dispersive-wave emission in compact hollow capillary systems," Opt. Lett. **44**, 2990–2993 (2019).

[52] C. Brahms, D. R. Austin, F. Tani, A. S. Johnson, D. Garratt, J. C. Travers, J. W. Tisch, P. S. Russell, and J. P. Marangos, "Direct characterization of tuneable few-femtosecond dispersive-wave pulses in the deep UV," Opt. Lett. **44**, 731–734 (2019).

[53] F. Belli, A. Abdolvand, J. C. Travers, and P. S. J. Russell, "Highly efficient deep UV generation by four-wave mixing in gas-filled hollow-core photonic crystal fiber," Opt. Lett. **44**, 5509–5512 (2019).

[54] K. C. Vishnubhatla, N. Bellini, R. Ramponi, G. Cerullo, and R. Osellame, "Shape control of microchannels fabricated in fused silica by femtosecond laser irradiation and chemical etching," Opt. Express **17**, 8685 (2009).

[55] V. Wanie, P. Barbato, J. Hahne, S. Ryabchuk, A. B. Wahid, D. Amorim, E. P. Månsson, A. Trabattoni, R. Osellame, R. Martínez Vázquez, and F. Calegari, "Ultraviolet supercontinuum generation using a differentially-pumped integrated glass chip," J. Phys. Photonics **6**, 025005 (2024).

[56] T. Harada, K. Takahashi, H. Sakuma, and A. Osyczka, "Optimum design of a grazing-incidence flat-field spectrograph with a spherical varied-line-space grating," Appl. Opt. **38**, 2743 (1999).

[57] L. Poletto, G. Naletto, and G. Tondello, "Grazing-incidence flat-field spectrometer for high-order harmonic diagnostics," Opt. Eng. **40**, 178–185 (2001).

[58] K. S. Budil, P. Salières, A. L'Huillier, T. Ditmire, and M. D. Perry, "Influence of ellipticity on harmonic generation," Phys. Rev. A **48**, 3437–3440 (1993).

[59] F. Ferrari, F. Calegari, M. Lucchini, C. Vozzi, S. Stagira, G. Sansone, and M. Nisoli, "High-energy isolated attosecond pulses generated by above-saturation few-cycle fields," Nat. Photonics **4**, 875–879 (2010).

[60] J. Bechhoefer, "Feedback for physicists: A tutorial essay on control," Rev. Mod. Phys. **77**, 783–836 (2005).

[61] V. Wanie, E. Bloch, E. P. Månsson, L. Colaizzi, S. Ryabchuk, K. Saraswathula, A. F. Ordonez, D. Ayuso, O. Smirnova, A. Trabattoni, V. Blanchet, N. Ben Amor, M.-C. Heitz, Y. Mairesse, B. Pons, and F. Calegari, "Capturing electron-driven chiral dynamics in UV-excited molecules," Nature **630**, 109–115 (2024).

[62] M. L. Murillo-Sánchez, A. Zanchet, S. Marggi Poullain, J. González-Vázquez, and L. Bañares, "Structural dynamics effects on the electronic predissociation of alkyl iodides," Sci. Rep. **10**, 6700 (2020).

[63] K. F. Chang, H. Wang, S. M. Poullain, J. González-Vázquez, L. Bañares, D. Prendergast, D. M. Neumark, and S. R. Leone, "Conical intersection and coherent vibrational dynamics in alkyl iodides captured by attosecond transient absorption spectroscopy," J. Chem. Phys. **156**, 114304 (2022).

[64] E. M. Warne, B. Downes-Ward, J. Woodhouse, M. A. Parkes, E. Springate, P. A. Pearcy, Y. Zhang, G. Karras, A. S. Wyatt, R. T. Chapman, and R. S. Minns, "Photodissociation dynamics of methyl iodide probed using femtosecond extreme ultraviolet photoelectron spectroscopy," Phys. Chem. Chem. Phys. **22**, 25695–25703 (2020).

[65] K. F. Chang, M. Reduzzi, H. Wang, S. M. Poullain, Y. Kobayashi, L. Barreau, D. Prendergast, D. M. Neumark, and S. R. Leone, "Revealing electronic state-switching at conical intersections in alkyl iodides by ultrafast XUV transient absorption spectroscopy," Nat. Commun. **11**, 4042 (2020).

[66] S. L. Cousin, F. Silva, S. Teichmann, M. Hemmer, B. Buades, and J. Biegert, "High-flux table-top soft x-ray source driven by sub-2-cycle, CEP stable, 185-$\mu$m 1-kHz pulses for carbon K-edge spectroscopy," Opt. Lett. **39**, 5383 (2014).

[67] S. M. Teichmann, F. Silva, S. L. Cousin, M. Hemmer, and J. Biegert, "0.5-keV Soft X-ray attosecond continua," Nat. Commun. **7**, 11493–11496 (2016).

[68] E. P. Månsson, S. L. Sorensen, C. L. Arnold, D. Kroon, D. Guénot, T. Fordell, F. Lépine, P. Johnsson, A. L'Huillier, and M. Gisselbrecht, "Multipurpose two- and three-dimensional momentum imaging of charged particles for attosecond experiments at 1 kHz repetition rate," Rev. Sci. Instrum. **85**, 123304 (2014).

[69] L. Rading, J. Lahl, S. Maclot, F. Campi, H. Coudert-Alteirac, B. Oostenrijk, J. Peschel, H. Wikmark, P. Rudawski, M. Gisselbrecht, and P. Johnsson, "A versatile velocity map ion-electron covariance imaging spectrometer for high-intensity XUV experiments," Appl. Sci. **8**, 998 (2018).